Angewandte Chemie
Eine Zeitschrift der Gesellschaft Deutscher Chemiker

Supporting Information

69451 Weinheim, Germany

A Nickel-Alkyl Bond in an Inactivated State of the Enzyme Catalyzing Methane Formation

Dariush Hinderberger, Rafal P. Piskorski, Meike Goenrich, Rudolf K. Thauer, Arthur Schweiger,[†] Jeffrey Harmer,[*] and Bernhard Jaun[*]

[*] Dr. D. Hinderberger, Prof. Dr. A. Schweiger,[†] Dr. J. Harmer
Laboratory of Physical Chemistry, Department of Chemistry and Applied Biosciences, ETH Zurich, 8093 Zurich, Switzerland
e-mail: harmer@phys.chem.ethz.ch

[*] Dr. R. P. Piskorski, Prof. Dr. B. Jaun
Laboratory of Organic Chemistry, Department of Chemistry and Applied Biosciences, ETH Zurich, 8093 Zurich, Switzerland
e-mail: jaun@org.chem.ethz.ch

Dr. M. Goenrich, Prof. Dr. R. K. Thauer
Max Planck Institute for Terrestrial Microbiology, Department of Biochemistry, Karl-von-Frisch-Straße, 35043 Marburg, Germany

[†] deceased on 4 January 2006

A. Materials and Methods.

Sample preparation.

Purification of MCR in the red1c state. *Methanothermobacter marburgensis* (DSM 2133, Deutsche Sammlung von Mikroorganismen und Zellkulturen, Braunschweig, Germany) was grown at 65 °C in a 10-L scale, as described previously.[S1] When a ΔOD_{578} of 4.5 was reached, the gas supply was switched from 80% H_2/20% CO_2/0.1% H_2S to 100% H_2 for 30 min to induce the EPR signals MCR_{red1} and MCR_{red2} in the cells. After 30-min incubation, the cells were cooled in a 15-min periode to 10 °C under continuous H_2 flow and then harvested anaerobically by centrifugation using a flow-through centrifuge (Hettich, centrifuge 17 RS). From the obtained wet cells (~80 g) the purification of MCR isoenzyme I[S2, S3] in the MCR_{red1} state was performed in an anaerobic chamber (Coy Instruments) filled with 95% N_2/5% H_2, as described.[S1] All buffers used during purification contained 10 mM coenzyme M (2-mercaptoethanesulfonate) (Merck, Darmstadt, Germany). The MCR_{red2} signal was lost due to the removal of coenzyme B. This method generally yielded 150 mg active MCR_{red1c} (in 3-4 ml) with 0.8-0.9 spins per nickel.

The protein concentration was determined by measuring the absorbance difference of oxidized enzyme (MCR_{silent}) at 420 nm using an ε = 44,000 $M^{-1}cm^{-1}$ for a molecular mass of 280,000 Da.

Synthesis of ammonium [3-^{13}C]-bromopropanesulfonate (^{13}C-BPS) and 3-hydroxypropane-1-sulfonate

Tetraethylammonium [^{13}C]-cyanate ([^{13}C]-1) was prepared from potassium [^{13}C]-cyanide according to the method described in Reference S4.

Tetraethylammonium [3-^{13}C]-2-cyanoethanesulfonate ([3-^{13}C]-2). 6.33 g sodium bromoethanesulfonate (30 mmol) was dissolved in 20 mL water, acidified with Amberlite IR-120, filtered, treated with 40% aqueous tetraethylammonium hydroxide solution to pH 7 and

lyophilized. The residue was dissolved in 9 mL DMSO, added to a suspension of 5.28 g [^{13}C]-**1** (33.6 mmol) in 9 mL DMSO and kept at 130 °C under nitrogen for 4 h.[S5] A white solid which crystallized after cooling overnight in 4 °C was filtered off and the product was precipitated from DMSO solution with acetone, followed by centrifugation, decantation and drying, giving 4.93 g (62%) of a white solid. ^{1}H NMR (400 MHz, D_2O): δ 1.03 (split *t*, $^{2}J_{CH}$ = 14.61, $^{3}J_{NH}$ = 3.79, 12 H), 2.70 (*q*, 2 H), overlapping 2.98 (*q*, 2 H) and 3.01 (*q*, 8 H). ^{13}C NMR (100 MHz, D_2O): δ 6.60, 13.51, 45.79, 51.94, 119.57. ESI-MS: *m/z* 293.0 (10), 135.2 (100), 81.3 (42).

Ammonium methyl [1-^{13}C]-3-sulfopropionate ([1-^{13}C]-3). A stirred solution of 4.47 g [3-^{13}C]-**2** (18 mmol) in 120 mL methanol was saturated with anhydrous HCl(g) while cooled on an ice-bath. The flask was capped with a septum and kept at -20 °C for 3 days and at RT for additional 4 days after which time it was evaporated to dryness under high vacuum using a double cooling trap, the first one filled with NaOH pellets.[S6] The crude product was dissolved in water, acidified with Amberlite IR-120, filtered, treated with cold conc. NH_3(aq) to pH 7 and lyophilized giving 2.64 g (79%) of a white solid. ^{1}H NMR (400 MHz, CD_3OD): δ 2.58 (*q*, 2 H), 2.79 (*q*, 2 H), 3.08 (*s*, 3 H). ^{13}C NMR (100 MHz, CD_3OD): δ 30.62, 31.20, 49.05, 174.05. ^{1}H NMR (400 MHz, D_2O): δ 2.58 (*q*, 2 H), 2.99 (*q*, 2 H), 3.12 (*s*, 3 H). ^{13}C NMR (100 MHz, D_2O): δ 29.32, 29.91, 46.36, 174.45. ESI-MS: *m/z* 359.2 (100), 198.0 (32), 168.2 (85), 119.6 (18).

Ammonium [3-^{13}C]-3-hydroxypropanesulfonate ([3-^{13}C]-4). Under nitrogen, 756 mg sodium borohydride (20 mmol) and 8 mL abs. diglyme were stirred in a round-bottom 2-neck flask until dissolution; 1.736 g finely ground lithium bromide (20 mmol) was added and the mixture was stirred for additional 30 min. A suspension of 2.418 g [1-^{13}C]-**3** (13 mmol) in 20 mL diglyme was added to the reaction mixture and stirred at 110 °C for 4 h under nitrogen.[S7] After cooling to RT, 20 mL methanol and 20 mL water was added and the pH was adjusted to

11 with 1.0 M NaOH. After acidification with Amberlite IR-120 and filtration, 70 mL methanol was added and the resulting solution was evaporated to dryness. Addition and evaporation of methanol (70 mL) was repeated five times.[S8] Finally, the sample was dissolved in water, acidified with Amberlite IR-120, filtered, treated with cold conc. NH_3(aq) to pH 7 and lyophilized. The resulting white solid (1.49 g, 66%) contained 10% of the starting material [1-^{13}C]-**3** but was used for the next step without separation. ^{1}H NMR (400 MHz, D_2O): δ 1.75 (*m*, 2 H), 2.73 (*m*, 2 H), 3.68 (*sextet*, $^1J_{CH}$ = 143.82, 2 H). ^{13}C NMR (100 MHz, D_2O): δ 27.28, 48.46, 60.70. ESI-MS: *m/z* 168.2 (35), 140.2 (80), 81.2 (100), 79.2 (60).

Ammonium [3-^{13}C]-3-bromopropanesulfonate ([3-^{13}C]-BPS). 1.465 g [3-^{13}C]-**4** (containing 10% [1-^{13}C]-**3**; 8.3 mmol [3-^{13}C]-**4**) and 100 mL aqueous hydrobromic acid (48%) were stirred at 130 °C for 3 h under nitrogen.[S9] The reaction mixture was evaporated to dryness, the solid off-white residue was dissolved in water, acidified with Amberlite IR-120 to pH 1, filtered, treated with cold conc. NH_3(aq) to pH 7 and lyophilized. [3-^{13}C]-BPS was isolated by chromatography on silica gel with 2-propanol-water-conc. NH_3 (8:1:1) as an eluent yielding 1.321 g of a white solid (67%), which still contained some [3-^{13}C]-**4** (< 5%). The isotopic purity of [3-^{13}C]-BPS as based on ^{1}H NMR was > 98.0%. ^{1}H NMR (400 MHz, D_2O): δ 2.08 (*m*, 2 H), 2.83 (*m*, 2 H), 3.38 (*sextet*, $^1J_{CH}$ = 153.91 Hz, 2 H). ^{13}C NMR (100 MHz, D_2O): δ 27.45, 32.05, 49.20. ESI-MS: *m/z* 204.1 (96), 202.0 (100), 81.2 (94), 79.2 (92).

Preparation of MCR_{BPS} and EPR-spectroscopic control. To induce the MCR_{BPS} state, the purified MCR was concentrated to approximately 1.5 ml (~100 mg/ml) using Amicon© Ultra Centrifugal Filter Devices (Millipore, Schwalbach, Germany) with a 100-kDa molecular mass cut-off. The concentrated MCR_{red1c} was supplemented with either 12.5 mM of 3-bromopropanesulfonic acid (Sigma-Aldrich, Steinheim, Germany) or 18 mM of [3-^{13}C]-bromopropanesulfonic acid. The convertion of MCR_{red1} to MCR_{BPS} was verified for completeness by X-band (9.44 GHz) CW EPR spectroscopy. Samples were diluted one to ten (10 mg/ml) with 10 mM Tris/HCl pH 7.6 in 0.3 cm (inner diameter) quartz tubes with 95%

N_2/5% H_2 as gas phase and closed with a closed off rubber tube. Initial EPR spectra to verify the induction of MCR_{BPS} were recorded with a Bruker EMX-6/1 EPR spectrometer at 77 K with a field modulation of 100 kHz (not shown).

B. EPR Spectroscopy

EPR spectroscopy The W-band (94.1653 GHz) CW-EPR spectrum (Fig. S1) was measured at 80 K on a Bruker E680 spectrometer with an mw power of 0.1 mW, a modulation amplitude of 0.7 mT, and a modulation frequency of 100 kHz. The field was calibrated using the two central lines from a CaO sample containing manganese ions.

The pulse EPR experiments were carried out at Q-band (35.3 GHz) on a home-built instrument[S10] and at X-band (9.7 GHz) on a Bruker E580 spectrometer. Both instruments were equipped with a Helium gas-flow cryostat from Oxford Inc. The field-swept frozen-solution EPR spectra (Q-band, temperature 20 K) were recorded by integrating over the echoes created with the pulse sequence $\pi/2$-τ-π-τ-*echo*, with pulse lengths $t_{\pi/2}$ = 50 ns, t_π = 100 ns, and an incremented interpulse delay of τ = 300 ns – 492 ns. The recorded spectra at each interpulse delay were added together. At X-band, FID-detected frozen-solution spectra were recorded by integration over the FID after a single pulse of 500 ns.

The first derivatives of these spectra were calculated numerically. The $^{14}N/^{13}C$ Davies-ENDOR spectra were measured at Q-band with the pulse sequence π-*T*-$\pi/2$-τ-π-τ-*echo,* with pulses of length $t_{\pi/2}$ = 40 ns and t_π = 80 ns, and τ = 300 ns. A radio-frequency pulse of length 13.5 μs and variable frequency ν_{ENDOR} was applied during time *T*. The ^1H Davies-ENDOR spectra were measured at Q-band with pulses of length $t_{\pi/2}$ = 40 ns and t_π = 80 ns, τ = 300 ns, and a radio frequency pulse of length 8.5 μs.

HYSCORE experiments employed the pulse sequence $\pi/2-\tau-\pi/2-t_1-\pi-t_2-\pi/2-\tau$–*echo.* At Q-band the following parameters were used: mw pulses of lengths $t_{\pi/2} = t_\pi$ = 16 ns, starting times 96 ns for t_1 and t_2, and time increments Δt = 16 ns or 12 ns (data matrix 256 × 256). Spectra

with different τ values were recorded. At X-band the parameters were: mw pulses of lengths $t_{\pi/2} = t_{\pi} = 16$ ns, starting times 96 ns for t_1 and t_2, $\Delta t = 16$ ns (data matrix 512 × 512). An eight-step phase cycle was used to remove unwanted echoes. The HYSCORE data were processed with MATLAB 6.5 (The MathWorks, Inc.). The time traces were baseline corrected with an exponential, apodized with a Gaussian window and zero filled. After a two-dimensional Fourier transformation absolute-value spectra were calculated. Spectra recorded with different τ values were added to eliminate τ-dependent blind spots.

EPR Simulations. The EPR and Davies-ENDOR spectra were simulated with the program *EasySpin*.[S11] HYSCORE spectra were also simulated with *EasySpin*, or, if only the cross-peak frequencies (and not the intensities) were of interest, by exact diagonalization of the spin Hamiltonian. Simulated spectra were generally fitted to experimental spectra using the Newton-Gauss-Levenberg/Marquardt (NGL/M) algorithm. To help find the global minimum, the NGL/M algorithm was used in conjunction with a large set of initial guesses, and the best fit was then found.

EPR Theory. The spin Hamiltonian for an $S = ½$ system coupled to i nuclei, in frequency units, is given by

$$H = (\beta_e/h)\mathbf{S}\mathbf{g}\mathbf{B}_o + \Sigma\, \mathbf{S}\mathbf{A}_i\mathbf{I}_i - (\beta_n/h)\Sigma\, g_{i,n}\mathbf{I}_i\mathbf{B_0} + \Sigma\, \mathbf{I}_i\mathbf{Q}_i\mathbf{I}_i\,, \qquad \text{(S1)}$$

where the terms describe the electron Zeeman interaction, the hyperfine interactions, the nuclear Zeeman interactions, and the nuclear quadrupole interactions (for nuclei with $I>1/2$). The ENDOR spectrum of a nucleus with spin $I = 1/2$ at a single orientation consists of two transitions. For $\mathbf{B}_0$ along one of the hyperfine principal axes the frequencies are given by $\nu = \left|\nu_I \pm \tfrac{1}{2}A_i\right|$, where ν_I is the nuclear Zeeman frequency and A_i is one of the principal hyperfine values. A HYSCORE spectrum contains cross-peak between the nuclear frequencies in one electron spin manifold with the nuclear frequencies in the other electron spin manifold. Generally, only a few of all possible cross-peaks are observed.

The point-dipole model. For protons, the dipolar part $\mathbf{A}_{\text{dip}}$ of the hyperfine interaction can be calculated using the point-dipole model[S12]

$$\mathbf{A}_{\text{dip}} = \mathbf{g}/g_e \sum_k \rho_k \mathbf{T}_k \tag{S2}$$

with

$$\mathbf{T}_k = \left(\mu_o/4\pi h\right)\left(g_e\beta_e g_n\beta_n\right)(3\mathbf{n}_k\mathbf{n}_k^{\dagger} - \mathbf{1})\frac{1}{r_k^3}, \tag{S3}$$

where r_k are the distances and $\mathbf{n}_k$ are the direction vectors between the protons (γ1 or γ2, β1 or β2) and nuclei k (Ni, ^{13}C, and N) with spin populations ρ_k. If the interactions matrix is axial, then $\mathbf{T}_k$=[-T, -T, 2T].

Calculation of spin populations from the isotropic and the dipolar parts of the ^{13}C hyperfine couplings. The isotropic hyperfine coupling is a direct measure of the spin population in s-type orbitals ρ_s, whereas the anisotropic part T of the hyperfine coupling allows for the calculation of the spin population in p-type orbitals ρ_p.[S13] For an unpaired electron (free electron, g_e=2.0023) on a ^{13}C-nucleus with a spin population of ρ_s=1 in an s-type orbital one would observe an isotropic hyperfine coupling constant of a_0=3777 MHz. If the electron resides in a p-type orbital one would observe a uniaxial hyperfine constant of b_0=107.3 MHz. Including a correction for the difference in the g values (g_{iso}(MCR$_{BPS}$)=2.1463), the spin populations in s-type and p-type orbitals can thus be estimated as:

$$\rho_s = \frac{A_{iso}}{a_0}\frac{g_e}{g_{iso}} = \frac{27MHz}{3777MHz}\frac{2.0023}{2.1463} \approx 0.7\% \tag{S4}$$

$$\rho_p = \frac{T}{b_0}\frac{g_e}{g_{iso}} = \frac{7MHz}{107.3MHz}\frac{2.0023}{2.1463} \approx 6\% \tag{S5}$$

Note that the value used for T in the calculation of ρ_p has been corrected for the through space dipolar interaction between the magnetic moment of $^{13}C_\gamma$ and spin population that is *located on the nickel center*. Assuming a nickel-carbon distance of 0.2 nm and 75% spin population

on the nickel, the contribution to the ^{13}C-hyperfine matrix is estimated as **T**=[-2, -2, 4] MHz, so that $T_{Ni\text{-}C}$=2 MHz. The corrected value was used ito estimate ρ_p and is thus given by: $T=T_{complete}- T_{Ni\text{-}C}$ = 9 MHz-2 MHz=7 MHz.

Detailed Analysis of the proton hyperfine couplings. Both geometric and electronic structural information can be obtained from the proton hyperfine matrices (See Figure 3a in the main text). Spin delocalization and spin polarization (from σ- and π-interactions) from the C_γ can contribute to the isotropic part, A_{iso}. Since the carbon contributes essentially only a p_z-orbital to the SOMO, the σ-type interactions are negligible and the isotropic hyperfine interaction of the protons on the propane sulfonate moiety may be described by

$$A_{iso}=B(\cos^2\theta)\rho(C_\gamma) \qquad \text{(S6)}$$

where B is a constant (~140 MHz for carbon atoms in alkyl radicals)[S14, S15], $\rho(C_\gamma)$ is the π-spin population on the γ-carbon and θ is the dihedral angle between the π-orbital on C_γ and the C-H bond of the corresponding proton.[S15]

The dipolar part of the proton hyperfine coupling is a through space interaction and is very sensitive to the unpaired electron-proton distance. In the point-dipole approximation[17,19] the dipolar hyperfine coupling A_{dip} shows a $1/r^3$-dependence on the electron-proton distance (see Equations S2 and S3).

The protons $H_{\gamma1}$ and $H_{\gamma2}$ show the characteristics of protons of a γ-CH_2 group that is coordinated to the nickel center. Both have small isotropic hyperfine values ($|A_{iso}|\leq$1.6 MHz), which is consistent with the proposed near-planar conformation of this terminal methylene group due to its near sp^2-hybridization. The two hydrogen atoms are situated in the plane where the non-hybridized p-orbital (with most of the ~6% carbon spin population) has a node and thus very little overlap with the hydrogen 1s-orbitals (θ≈90° in Eq. S6). On the other hand, they are in close proximity to the nickel ion and the C_γ, on which the main part (Ni: ~75%, C_γ: ~(6+0.7)%) of the unpaired electron spin population is located (the remainder of

the spin population is distributed e.g. to the macrocycle nitrogens). An estimate of the expected dipolar hyperfine coupling of the γ-protons using the multi-center point-dipole model (r(Ni-$H_{\gamma1}$)=0.21 nm, r(Ni-$H_{\gamma2}$)=0.21 nm, r(C-H_{γ})=0.1 nm, r(Ni-C_{γ})=0.2 nm, ρ_{Ni}=0.75, $\rho_{C\gamma}$=0.06) yields principal values that are in good agreement ($T_{calculated} \approx T_{experimental} \approx 6$ MHz) with the experimental data and our interpretation. The fact that the hyperfine couplings for the two γ-protons are slightly inequivalent can be explained as a consequence of the tilt angle of ~20° for the Ni-C bond, which decreases the coordination symmetry as compared to an exactly axial coordination of the ligand.

We assign the large isotropic hyperfine coupling, which requires an efficient orbital overlap for the transfer of unpaired electron spin population, to the proton $H_{\beta1}$ (Figure 3a). The hyperfine coupling of the second proton $H_{\beta2}$ is not resolved in the spectra and contributes only to the "matrix line", which is composed of signals from many weakly coupled protons surrounding the Ni-center. The striking difference in the isotropic hyperfine couplings of the two β-protons can be consistently explained as a consequence of the near sp^2-hybridization of the coordinated C_{γ} and the sp^3-hybridization of C_{β}. The range of possible dihedral angles $\theta_{\beta1}$ (∠Ni-C_{γ}-C_{β}-$H_{\beta1}$) can be calculated from Eq. S6 using the angular constraint $\theta_{\beta2} = \theta_{\beta1}+120°$, the isotropic hyperfine coupling $A_{iso}(H_{\beta1})$=15 MHz, and an upper limit for $A_{iso}(H_{\beta2}) \leq 4$ MHz (estimated limit for the couplings in the matrix proton range, see Fig. 2):

$$A_{iso}(H_{\beta2}) = A_{iso}(H_{\beta1}) \cos^2(\theta_{\beta1}+120°)/\cos^2(\theta_{\beta1}) \quad \text{(S7)}$$

When $A_{iso}(H_{\beta2})$ is plotted as a function of $\theta_{\beta1}$ (see Fig. S6) one finds that the range of angles for which $A_{iso}(H_{\beta2}) \leq 4$ MHz is $0<\theta_{\beta1}<50°$ (see Fig 3b). From the dipolar part $\mathbf{A}_{dip}$ of the hyperfine matrix of $H_{\beta1}$, we estimate the Ni-$H_{\beta1}$ distance to be 0.27-0.29 nm. These data compare well with the angle and the distance determined from the crystal structure of $MCR_{ox1\text{-}silent}$ ($\theta_{\beta1}$=24°, r(Ni(II)-$H_{\beta1}$)=0.28 nm), where HS-CoM is coordinated to the Ni(II) ion via its thiol sulfur atom and the sulfonate group is anchored to the protein via hydrogen

bonding.[2] The β-CH_2 group of the propane sulfonate moiety in MCR_{BPS} adopts an orientation similar to that of the β-CH_2 group of HS-CoM in $MCR_{ox1\text{-}silent}$.

C. Figures and Tables.

Table S1: ^{14}N hyperfine coupling parameters used for Davies-ENDOR simulations

Figure S1: W-band (94.1 GHz) CW-EPR spectrum and simulation of MCR_{BPS}

Figure S2: Q-band (35.3 GHz) nitrogen (^{14}N) Davies-ENDOR of MCR_{BPS} and Q-band (35.3 GHz) carbon (^{13}C) Davies-ENDOR of ^{13}C-MCR_{BPS}

Figure S3: Q-band (35.3 GHz) HYSCORE of ^{13}C-MCR_{BPS}

Figure S4: Q-band (35.3 GHz) proton Davies-ENDOR of ^{13}C-MCR_{BPS}

Figure S5: X-band (9.75 GHz) HYSCORE of ^{13}C-MCR_{BPS}

Figure S6: Plot of Eq. 3: $A_{iso}(H_{\beta 2})$ as a function of $\theta(H_{\beta 1})$

Table S1.

MCR_{BPS} ^{14}N hyperfine and nuclear quadrupole couplings as determined from simulations of the experimental spectra.

Hyperfine and nuclear quadrupole coupling parameters were determined from simulations of pulse ENDOR data (Figure S2). Note that the hyperfine parameters are very similar to those found in MCR_{red1}.[S16] The Euler angles α, β, γ define the passive rotation of the hyperfine (A) or nuclear quadrupole (Q) principal axes systems into the g-matrix principal axes system, e.g. $\mathbf{A}=\mathbf{R}(\alpha, \beta, \gamma)\mathbf{A}_{diagonal}\,\mathbf{R}^{\dagger}(\alpha, \beta, \gamma)$. The nuclear quadrupole interactions are: $\kappa = (e^2qQ/h)/(4I(2I-1))$ and the asymmetry parameters $\eta = (Q_x-Q_y)/Q_z$ with $Q_x = -\kappa(1-\eta)$, $Q_y = -\kappa(1+\eta)$, and $Q_z = 2\kappa$.

	A_x (MHz)	A_y (MHz)	A_z (MHz)	A_{iso} (MHz)	α, β, γ (°)	$\lvert e^2qQ/h \rvert$ (MHz)	η	α, β, γ (°)
$^{14}N(1,3)$	34	27.7	29.7	30.5	45, 0, 0	2.4	0.33	45, 90, 0
$^{14}N(2,4)$	31	22.5	26.3	26.6	135, 0, 0	3.6	0.67	135, 90, 0

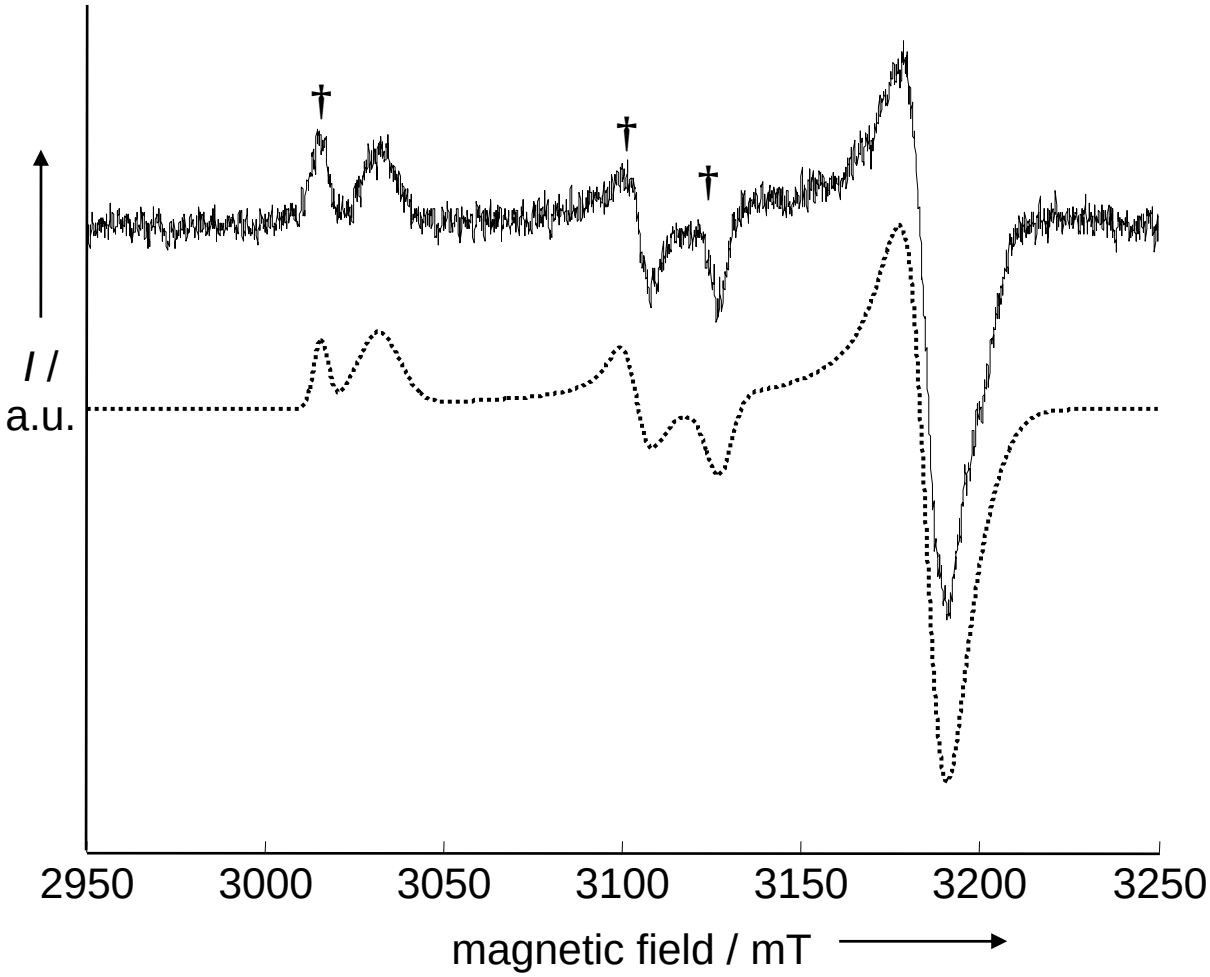

Figure S1.

CW-EPR spectrum of ^{13}C-MCR$_{BPS}$ (solid line) measured at W-band (94.1 GHz) and simulation (gray dotted line) with the g values given in Table 1. The crosses mark the MCR$_{ox1}$ signal, which is an inpurity in some MCR$_{red1}$ preparations.

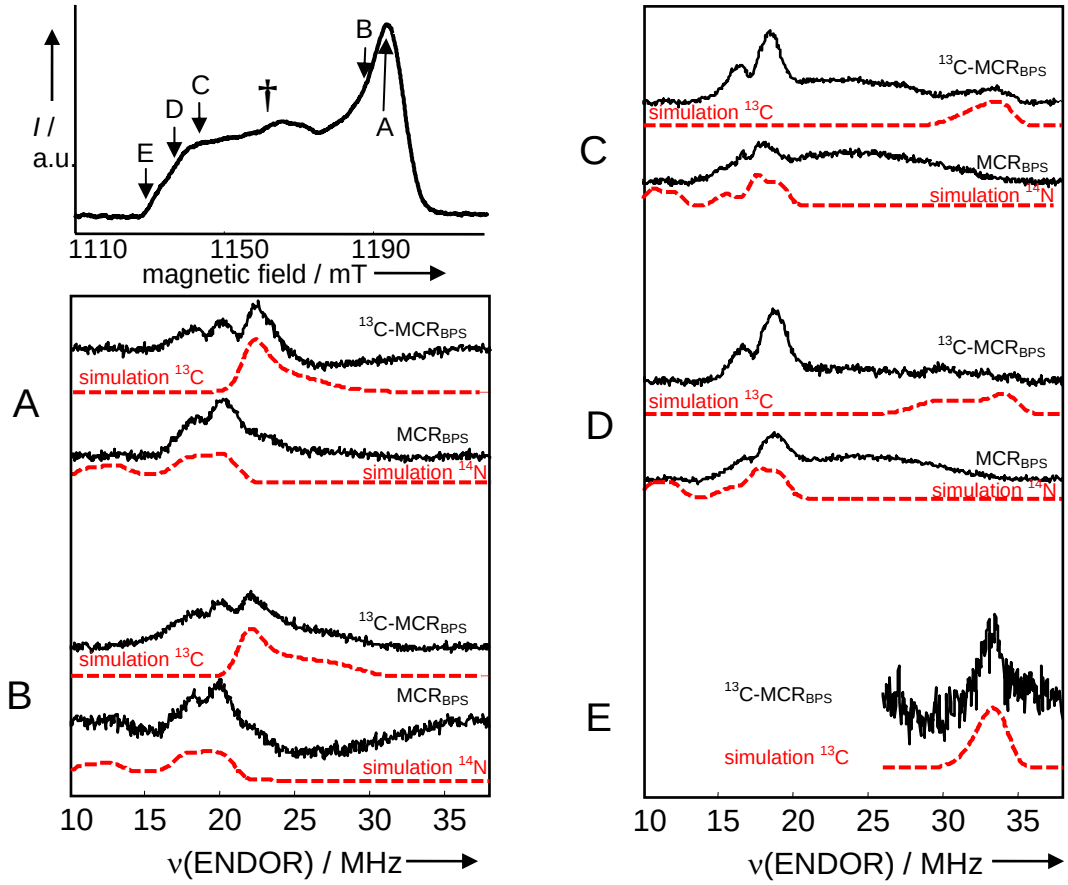

Figure S2.

Q-band (microwave frequency 35.3 GHz) EPR experiments on ^{13}C-MCR$_{BPS}$ and MCR$_{BPS}$. Upper left: Echo-detected field-swept EPR spectrum of ^{13}C-MCR$_{BPS}$. The cross indicates a small MCR$_{ox1}$ impurity ($g_{\perp}$-region). Arrows marked "A" to "E" show the field positions at which Davies-ENDOR experiments on both samples were performed. a)-e) Davies-ENDOR spectra of ^{13}C-MCR$_{BPS}$ (respective upper solid line), simulations of the $^{13}C_{\gamma}$-signals (upper dashed red line), Davies-ENDOR spectra of MCR$_{BPS}$ (respective lower solid line) and simulations of the hydropyrrolic ^{14}N-nuclei of F$_{430}$. Only the high-frequency peaks are shown. The hyperfine parameters used for the simulation of the nitrogen nuclei are very close to those found in MCR$_{red1}$ and are given in Table S1. The $^{13}C_{\gamma}$ hyperfine coupling parameters are presented in Table 1.

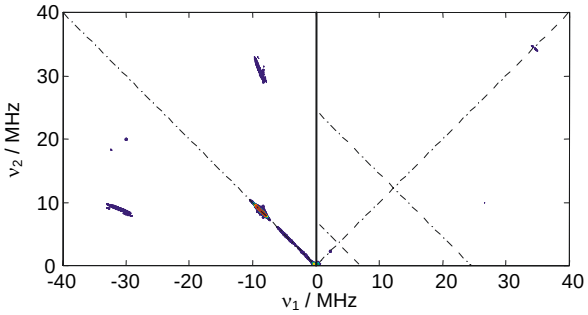

G exp.

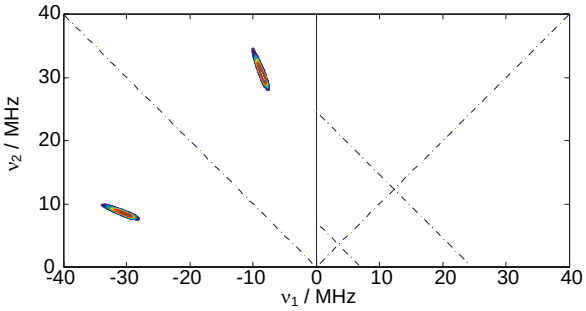

sim.

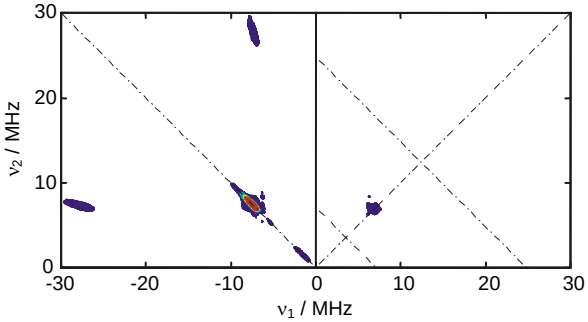

F exp.

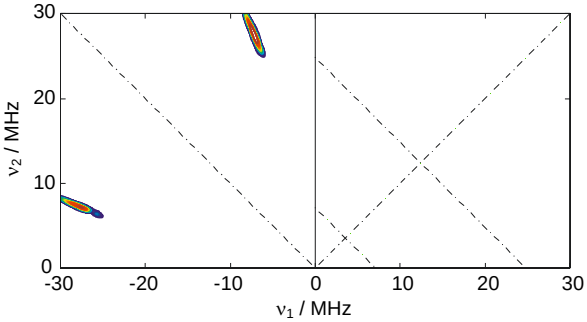

sim.

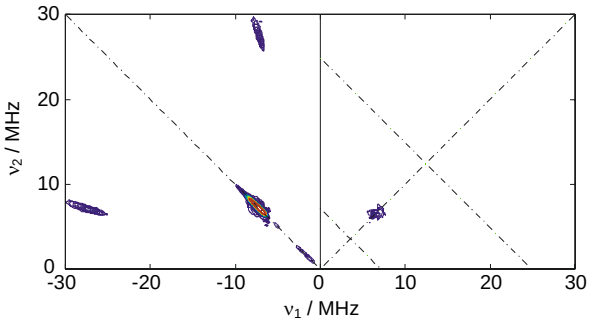

E exp.

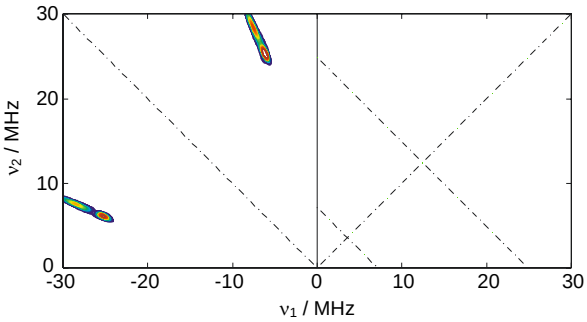

sim.

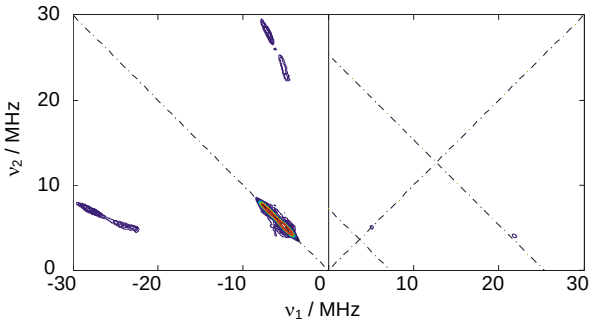

D exp.

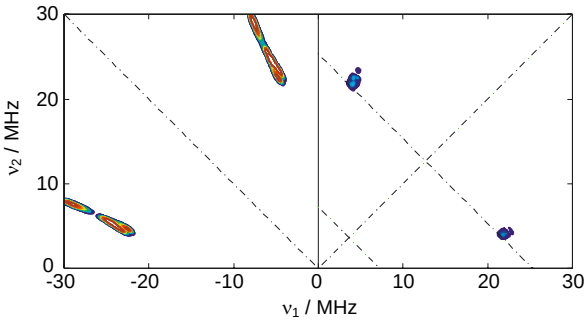

sim.

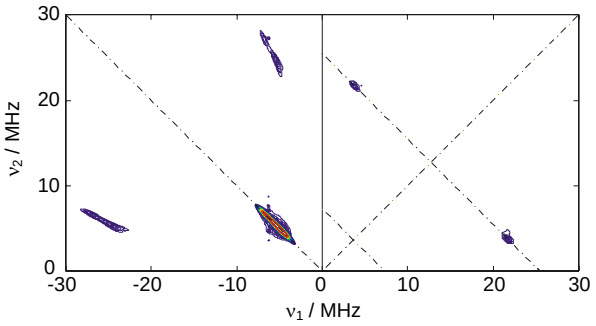

C exp.

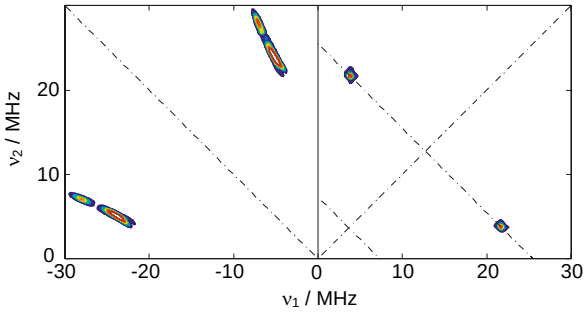

sim.

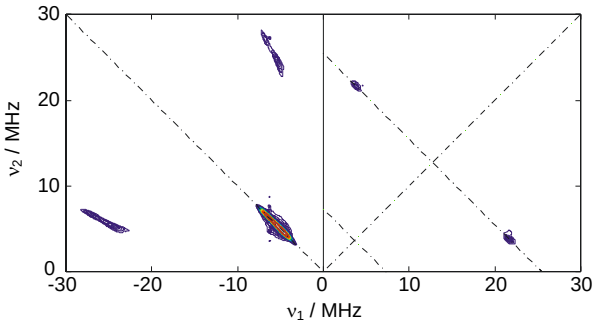

B exp.

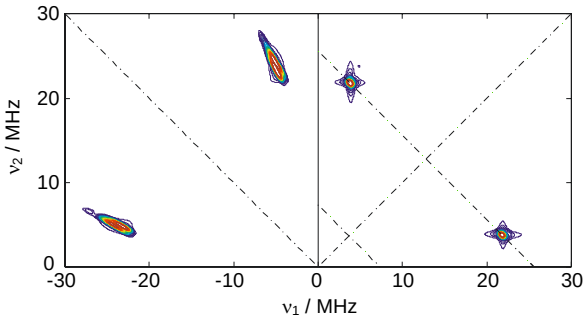

sim.

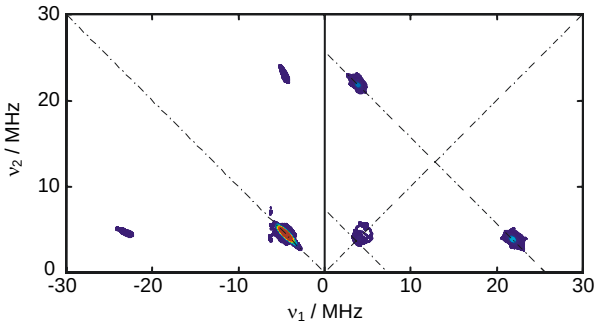

A exp.

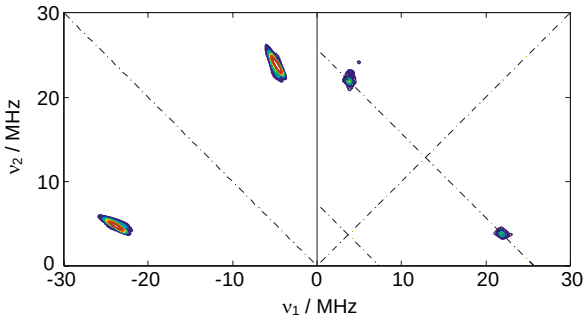

sim.

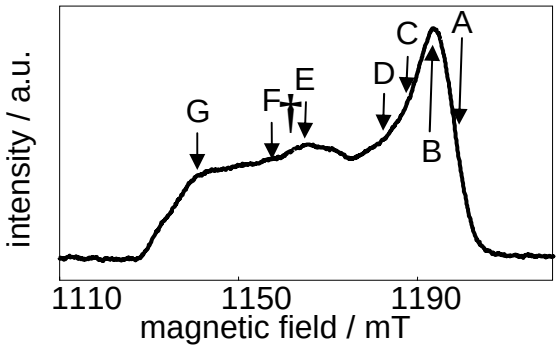

H

Figure S3.

Q-band (35.3 GHz) HYSCORE spectra of ^{13}C-MCR$_{BPS}$. a)-g) HYSCORE spectra showing $^{13}C_{\gamma}$ signals (left) and simulations using the $^{13}C_{\gamma}$ hyperfine parameters given in Table 1 (right) of the spectra at the respective positions in the field-swept EPR spectrum. Note that the diagonal peaks in the second quadrant are due to π-pulse non-ideality. h) Echo-detected field-swept EPR spectrum. The cross indicates the $g_{\perp}$ region of a small MCR$_{ox1}$ impurity.[19, 22]

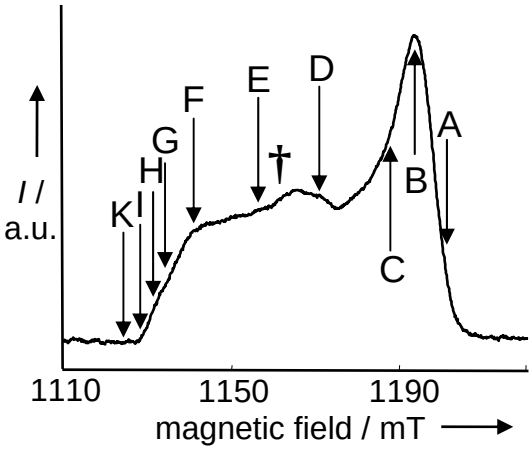
I /
a.u.
K
I
H
G
F
E
†
D
C
B
A
1110
1150
1190
magnetic field / mT

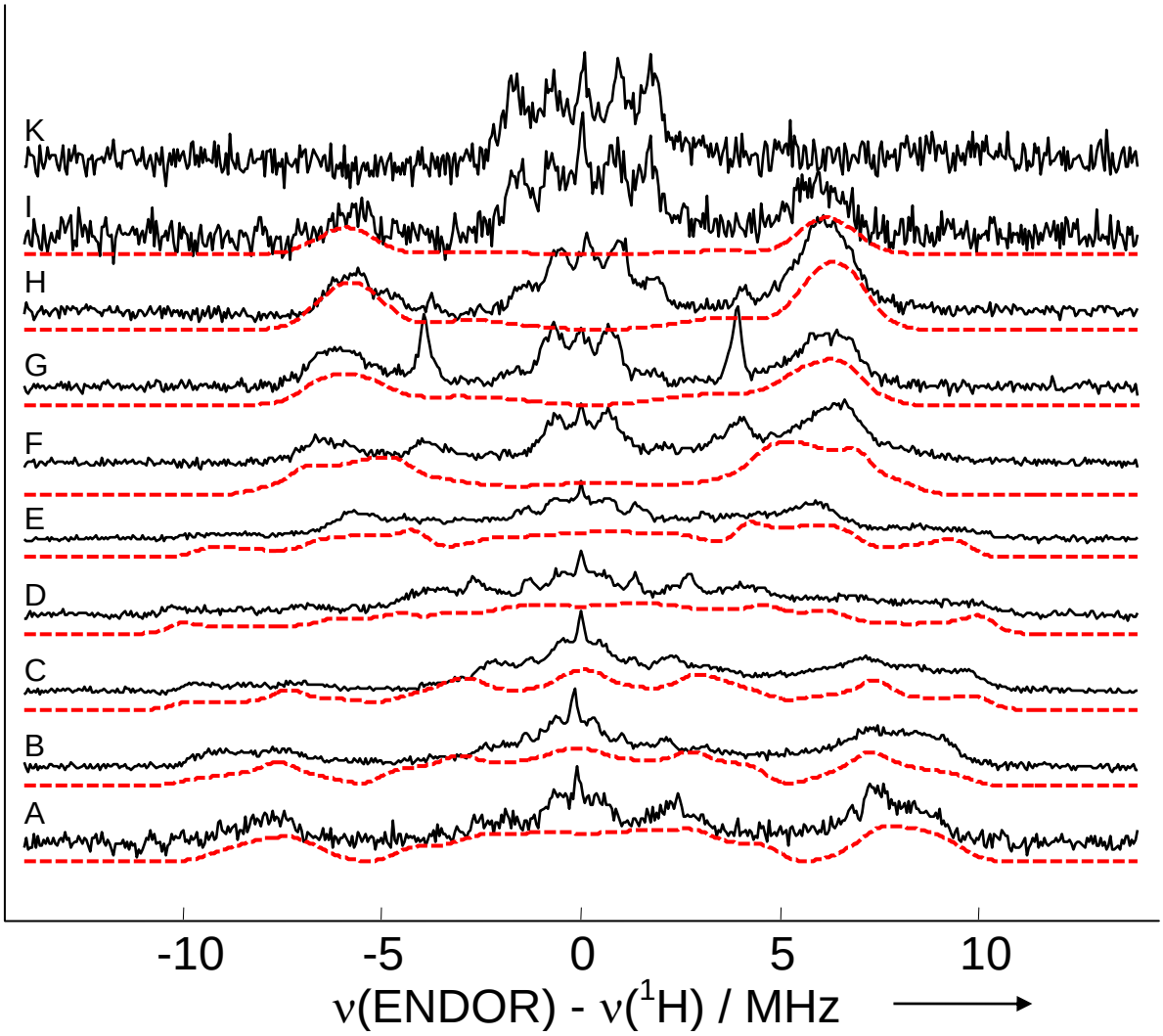
K
I
H
G
F
E
D
C
B
A
-10
-5
0
5
10
ν(ENDOR) - ν(1H) / MHz

Figure S4.

Q-band (35.3 GHz) proton Davies-ENDOR spectra of ^{13}C-MCR$_{BPS}$.

Upper left: Echo-detected, field-swept EPR spectrum of ^{13}C-MCR$_{BPS}$. The cross indicates a small MCR$_{ox1}$ impurity ($g_{\perp}$-region). Arrows marked "A" to "K" show the field positions at which Davies-ENDOR experiments on both samples were performed. a)-k) Davies-ENDOR spectra of ^{13}C-MCR$_{BPS}$ (respective upper solid line) and simulations of three ^{1}H nuclei (dashed red lines) using the hyperfine parameters presented in Table 1.

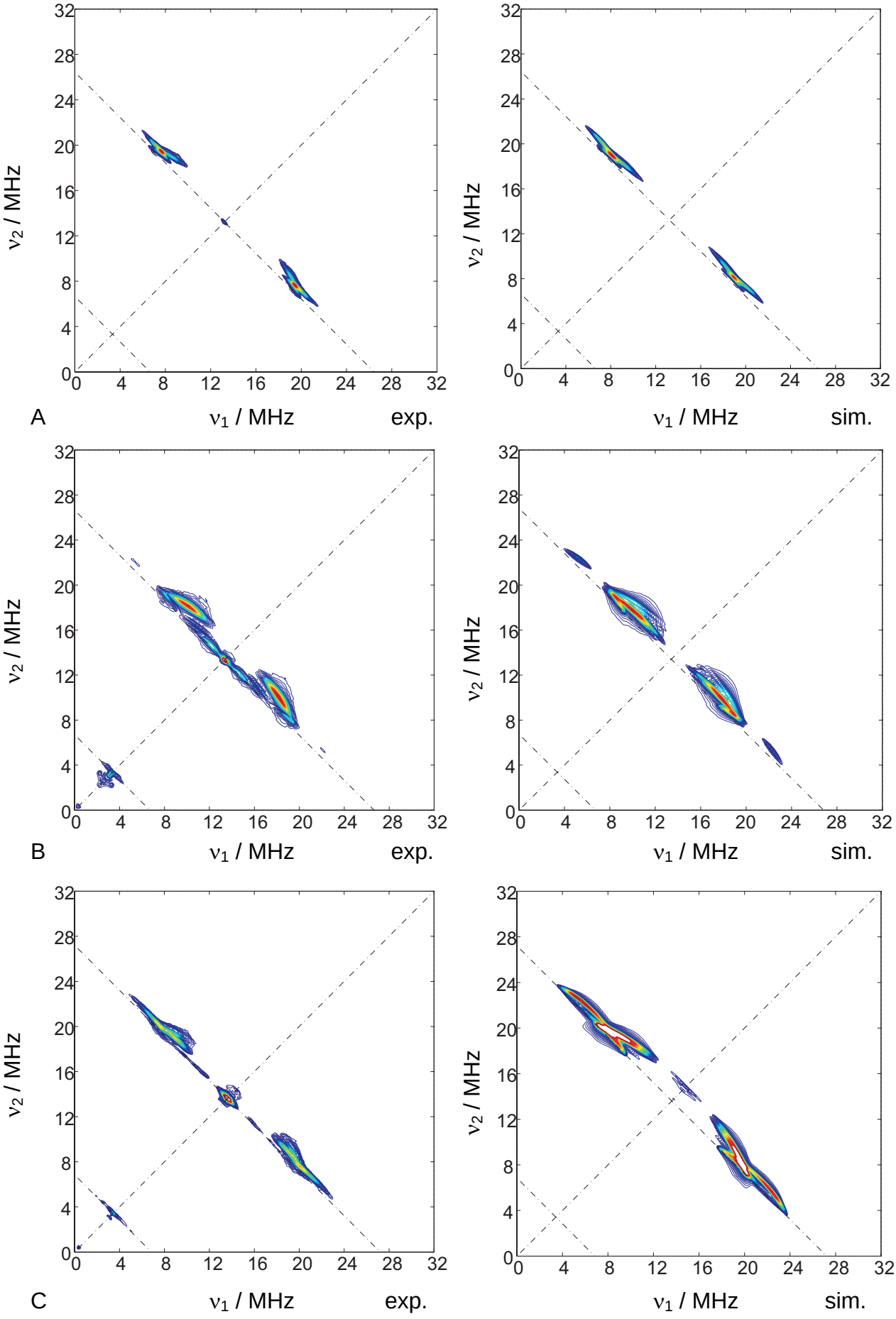
A
exp.
sim.
B
exp.
sim.
C
exp.
sim.
ν_1 / MHz
ν_2 / MHz
0
4
8
12
16
20
24
28
32

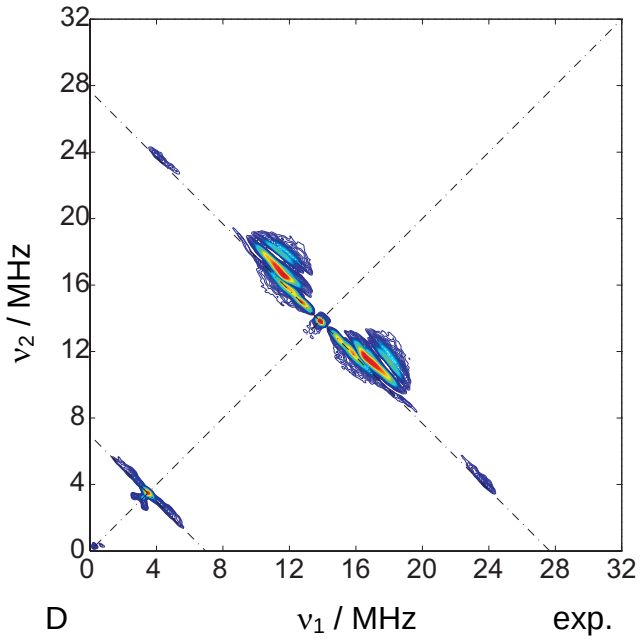

D exp.

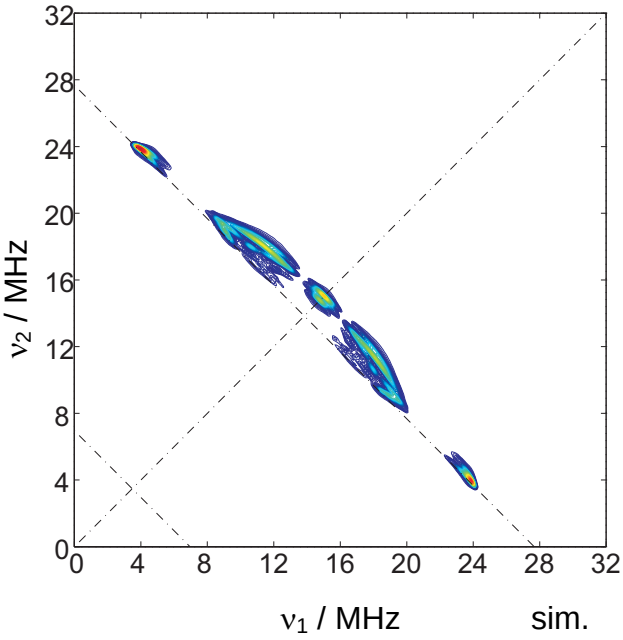

sim.

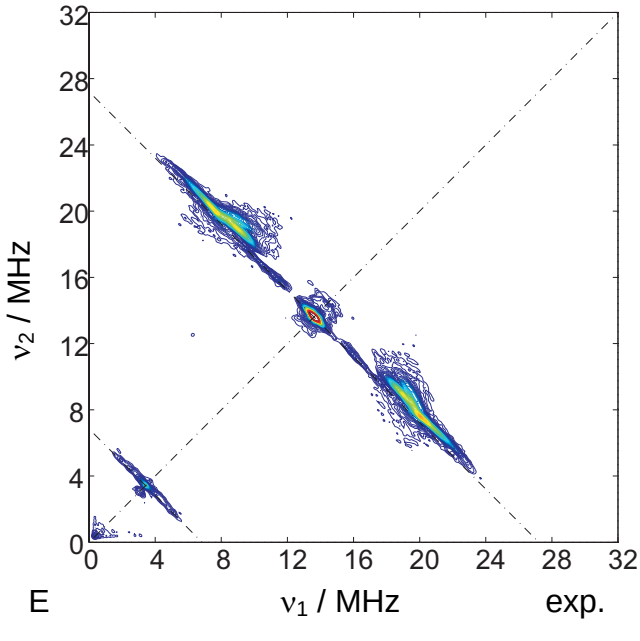

E exp.

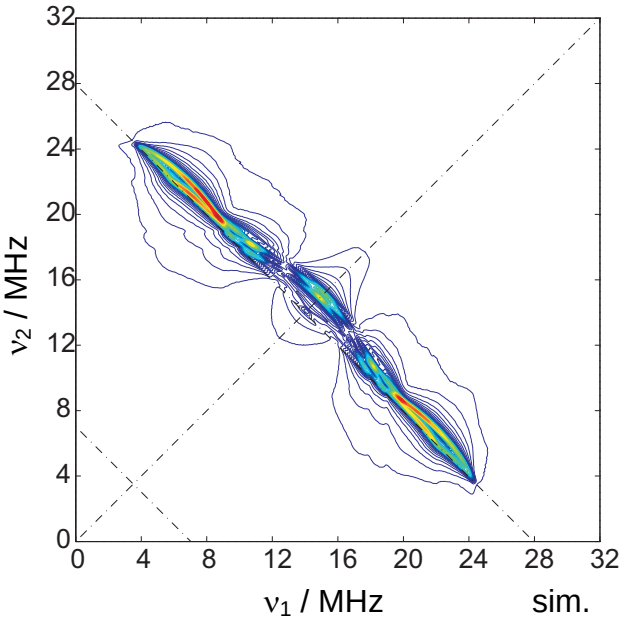

sim.

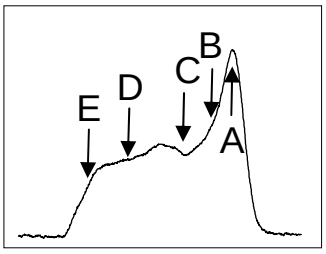

H

Figure S5.

X-band (9.7 GHz) HYSCORE spectra of ^{13}C-MCR$_{BPS}$. a)-g) HYSCORE spectra showing ^{1}H signals (left) and simulations using the ^{1}H hyperfine parameters given in Table 1 (right) of the spectra at the respective positions in the field-swept EPR spectrum. h) Echo-detected field-swept EPR spectrum.

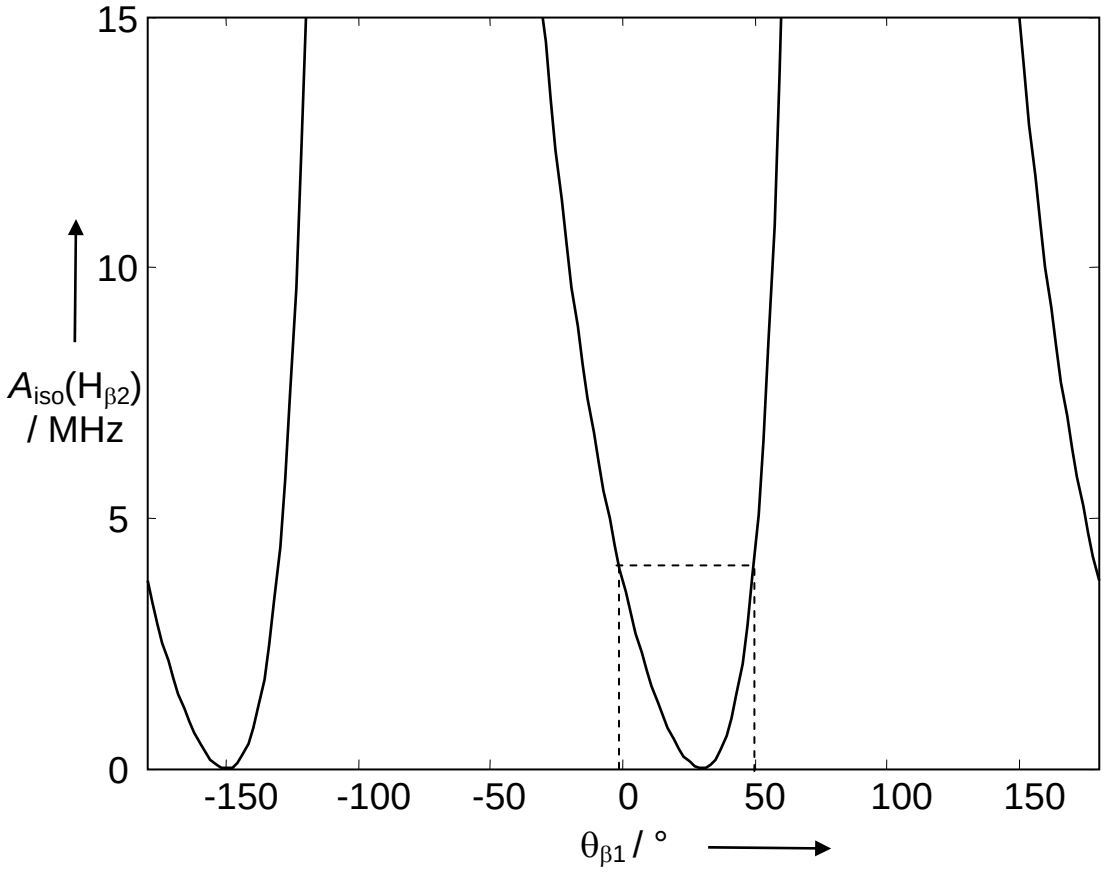

Figure S6.

Plot of $A_{iso}(H_{\beta 2})$ as a function of $\theta_{\beta 1}$, as described by Eq. S7. The range of angles for which $A_{iso}(H_{\beta 2}) \leq 4$ MHz is fulfilled is indicated by the dashed lines, $0<\theta_{\beta 1}<50°$. The second set of solutions (around -150°) can be excluded from the dipolar coupling of $H_{\beta 1}$, which indicates a distance of 0.28 nm. The solutions around -150° is only valid for Ni-$H_{\beta 1}$ distances that are much larger.

References

[S1] F. Mahlert, W. Grabarse, J. Kahnt, R.K. Thauer, E.C. Duin, *J. Biol. Inorg. Chem.* **2002**, *7*, 101

[S2] S. Rospert, D. Linder, J. Ellermann, R.K. Thauer, *Eur. J. Biochem.* **1990**, *194*, 871

[S3] L.G. Bonacker, S. Baudner, E. Mörschel, R. Böcher, R.K. Thauer, *Eur. J. Biochem.* **1993**, *217*, 587

[S4] C. Grundmann, in *Methoden der organischen Chemie (Houben-Weyl). Carbonsäuren und Carbonsäure-Derivate*; J. Falbe, Ed., Thieme, Stuttgart, New York, **1985**, p. 1318-1460.

[S5] H. Kobler, K.-H. Schuster, G. Simchen, *Liebigs Ann. Chem.* **1978**, 1946

[S6] A. Schwartz, P. Madan, *J. Org. Chem.* **1986**, *51*, 5463

[S7] H. C. Brown, E. J. Mead, B. S. C. Rao, *J. Am. Chem. Soc.* **1955**, *77*, 6209

[S8] K. B. Hicks, G. L. Simpson, A. G. W. Bradbury, *Carbohydr. Res.* **1986**, *147*, 39

[S9] P. Rumpf, *Bull. Soc. Chim. Fr.* **1938**, *5*, 871

[S10] I. Gromov, J. Shane, J. Forrer, R. Rakhmatoullin, Yu. Rozentzwaig, A. Schweiger, *J. Magn. Res.* **2001**, *149*, 196

[S11] see http:// www.esr.ethz.ch

[S12] A. Schweiger, G. Jeschke, *Principles of Pulse Electron Paramagnetic Resonance*, Oxford Univ. Press, Oxford, **2001**

[S13] J. A. Weil, J. R. Bolton, J. E. Wertz, *Electron Paramagnetic Resonance – Elementary Theory and Practical Applications*, Wiley, New York, **1994**

[S14] D. Lazdins, M. Karplus, *J. Chem. Phys.* **1966**, *44*, 1600

[S15] M. W. Werst, C. E. Davoust, B. M. Hoffman, *J. Am. Chem. Soc.* **1991**, *113*, 1533

[S16] J. Telser, Y. C. Horng, D. F. Becker, B. M. Hoffman, S. W. Ragsdale, *J. Am. Chem. Soc.* **2000**, *122*, 182